Journal of Sound and Vibration (1997) **199**(1), 17–31

STRAIN SENSING OF COMPOSITE PLATES SUBJECTED TO LOW VELOCITY IMPACT WITH DISTRIBUTED PIEZOELECTRIC SENSORS: A MIXED FINITE ELEMENT APPROACH

L. YIN AND Y. SHEN

Department of Engineering Mechanics, Xi'an Jiaotong University, Xi'an, Shaanxi, 710049, People's Republic of China

(*Received* 15 *August* 1995, *and in final form* 6 *May* 1996)

A mixed finite element formulation is presented for modelling the behaviour of laminated composite plates containing integral piezoelectric layers and is utilized to study the response of the distributed sensors made of PVDF film when the laminate is subjected to low velocity impact. The formulation is based on the Hamilton variational principle which takes into account the electric field potential energy of the piezoelectric layers. In view of the intrinsic state of the contact problem, the laminate is discretized by three-dimensional and two-dimensional elements, between which transition elements are introduced to provide a smooth interphase zone. Numerical examples show the accuracy of the method. The close circuit charge generated by the piezoelectric sensor is computed and the influence of the skew angle of the PVDF film is examined as well.

1. INTRODUCTION

Intelligent/smart structures featuring a network of integrated sensors and actuators within a host material will have a tremendous effect upon numerous industrial fields. The idea of applying "smart" materials to mechanical and structural systems has been studied by researchers in various disciplines. Among the promising materials with adaptable properties such as piezoelectric polymers and ceramics, shape memory alloys, electrorheological fluids and optical fibers, piezoelectric materials can be used both as sensors and actuators because of their high direct and converse piezoelectric effects. Consequently a great deal of effort has been devoted to developing integrated piezoelectric sensors and actuators in structural modal sensing, vibration and acoustic control as well as changing structures' geometries actively. The literature vividly demonstrates the effectiveness of piezoelectric sensors and actuators in a wide range of applications. Since piezoelectric sensors measure the average local strain over the area to which they are bonded [1, 2], further investigation concentrates on the methodology of using piezoelectric devices as sensors to monitor structural damage. This concept is exploited by Yin [3] in detecting edge delamination in composite plates caused by remote uniaxial loading.

Because of their weak impact resistance properties, laminated composite plates are very susceptible to damage when impacted by a foreign solid object. If the impacting velocity is high enough, the laminate will be perforated while in the low velocity case, severe damage can be induced in the composites. Since this damage is internal and cannot be easily detected from its appearance, to a certain degree, low velocity impact is more

0022–460X/97/010017 + 15 $25.00/0/sv960627

dangerous. Accordingly, numerous experimental and analytical techniques have been developed for composite plates subjected to low velocity impact. Some important aspects are briefly reviewed in the following.

Sun [4] and Ramkumar [5] predicted the history of a contact force analytically based on the transverse shear deformable plate theory—Mindlin's plate theory. Later Sun and Chen [6] investigated the effects of initial stresses on the laminates' low velocity dynamic response by means of two-dimensional finite elements also formulated by the Mindlin plate theory. In order to comprehend the laminates' response due to low velocity impact more thoroughly, Lee [7] proposed a three-dimensional finite element effort by utilizing eight node brick elements. With the same elements not including incompatible modes, Wu [8] developed the 3-D finite element analysis of the impact problem in detail. Recently Pojanasomboon [9] used fiber optic extrinsic Tabry Perot sensors to measure transient impact induced strain.

This investigation is undertaken to describe low velocity impact induced transient strain of composite laminates by applying distributed built-in piezoelectric sensors made from PVDF film. This is fulfilled by a mixed finite element approach. The concept of adopting different element grids in different regions according to their deformation and stress state has been successfully utilized in studying structures including shells [10] and edge delaminations in the free edges of laminates under remote uniform axial loading [11]. In the present study, after reviewing some experimental results in the literature [12, 13], the laminate is modelled by three-dimensional elements in the possible damage area around the impact point while the rest of the plate is discretized by two-dimensional plate elements. Between these two regions, a transition area consisting of two kinds of transition elements is introduced to connect these two regions smoothly. In addition, the piezoelectric patches are divided by the 3-D elements or 2-D elements depending on their locations. With this idealization, it is possible to analyze the transient dynamics of composite plates including piezoelectric layers incited by foreign low velocity impact with much less computational effort compared to the complete three-dimensional idealization. The calculated charge generated by the piezoelectric sensors shows that these sensors are effective in monitoring transient impact induced strain.

2. BASIC EQUATIONS

Consider a flat composite plate with incorporated piezoelectric layers impacted by a solid object of mass m_s (see Fig. 1). Under the assumptions that the impactor is spherical and the contact is a point one, the equation of the impactor's motion is expressed by Newton's second law as:

$$m_s \ddot{w}_s = F_s, \tag{1}$$

where w_s is the impactor's displacement, F_s is the contact force. For the laminate consisting of piezoelectric layers, Hamilton's variational principle in the absence of damping can be written as:

$$\delta \int_{t_1}^{t_2} (K - U + W)\, \mathrm{d}t = 0, \qquad K = \tfrac{1}{2} \int_V \rho \{\dot{\mathrm{u}}\}^{\mathrm{T}} \{\dot{\mathrm{u}}\}\, \mathrm{d}v, \qquad U = U_M + U_E,$$

$$U_M = \tfrac{1}{2} \int_V \{\varepsilon\}^{\mathrm{T}} \{\sigma\}\, \mathrm{d}v, \quad U_E = -\tfrac{1}{2} \int_{V_p} \{\mathrm{E}\}^{\mathrm{T}} \{\mathrm{D}\}\, \mathrm{d}v, \quad W = \int_{S_v} \{\mathrm{u}\}^{\mathrm{T}} \{\mathrm{T}\}\, \mathrm{d}s + \int_{S_Q} \Phi Q\, \mathrm{d}s, \tag{2}$$

where K is the kinetic energy, U is the potential energy including strain energy U_M and electric field potential energy U_E of the piezoelectric layers, and W is the work done by surface tractions $\{T\}$ and surface charge Q. $\{\mathrm{u}\}$, $\{\varepsilon\}$, $\{\sigma\}$, $\{\mathrm{E}\}$, $\{\mathrm{D}\}$ and Φ are displacement, strain, stress, electric field intensity, electric displacement vectors and voltage respectively. V is the volume of the laminate including piezoelectric layers, and V_p is the volume of the piezoelectric layers. If the non-linear terms are neglected, the linear constitutive equations of the piezoelectric materials can be written in the form:

$$\{\sigma\} = [\mathrm{C}]\{\varepsilon\} - [\mathrm{e}]^{\mathrm{T}}\{\mathrm{E}\}, \qquad \{\mathrm{D}\} = [\mathrm{e}]\{\varepsilon\} + [\xi]\{\mathrm{E}\}. \tag{3}$$

where [C] is material stiffness matrix, [ξ] is the permittivity matrix, and [e] is the piezoelectric stress/charge coefficient matrix:

$$[\mathrm{e}] = [\mathrm{d}][\mathrm{C}], \tag{4}$$

where [d] is the piezoelectric strain constants matrix. Let the electric variables be zero and equation (3) degenerates into the constitutive equations of composites. Substituting equation (3) into equation (2), the following can be obtained:

$$\int_{t_1}^{t_2} \left(\int_V (\rho\{\delta\mathrm{u}\}^{\mathrm{T}}\ddot{u} + \{\delta\varepsilon\}^{\mathrm{T}}[\mathrm{C}]\{\varepsilon\})\,\mathrm{d}v - \int_{V_p} (\{\delta\varepsilon\}^{\mathrm{T}}[\mathrm{e}]^{\mathrm{T}}\{\mathrm{E}\} + \{\delta\mathrm{E}\}^{\mathrm{T}}[\mathrm{e}]\{\varepsilon\} \right.$$

$$\left. + \{\delta\mathrm{E}\}^{\mathrm{T}}[\xi]\{\mathrm{E}\})\,\mathrm{d}v - \left(\int_{S_\sigma} \{\delta\mathrm{u}\}^{\mathrm{T}}\{\mathrm{T}\}\,\mathrm{d}s + \int_{S_Q} Q\delta\Phi\,\mathrm{d}s \right) \right) \mathrm{d}t = 0. \tag{5}$$

By introducing the new extended displacement, strain, stress and traction vectors, i.e.,

$$\{\bar{\mathrm{u}}\} = \begin{Bmatrix} u \\ \Phi \end{Bmatrix}, \qquad \{\bar{\varepsilon}\} = \begin{Bmatrix} \varepsilon \\ -E \end{Bmatrix}, \qquad \{\bar{\sigma}\} = \begin{Bmatrix} \sigma \\ D \end{Bmatrix}, \qquad \{\bar{\mathrm{T}}\} = \begin{Bmatrix} T \\ Q \end{Bmatrix}, \tag{6}$$

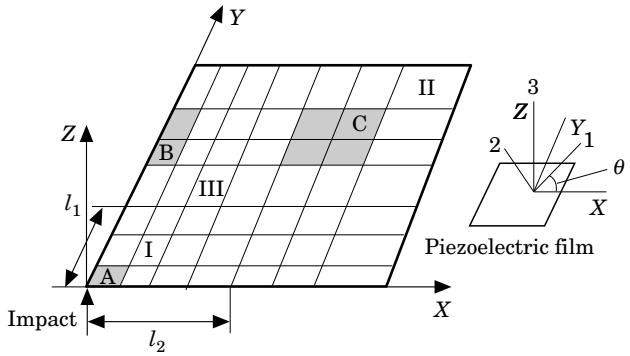

Figure 1. Geometry and finite element mesh: I, 3-D elements; II, transition elements; III, 2-D elements. A, sensor A; B, sensor B; C, sensor C.

equation (5) can be rewritten in a succinct form:

$$\int_{t_1}^{t_2}\left(\int_V (\rho\{\delta \mathrm{u}\}^{\mathrm{T}}\ddot{u} + \{\delta\bar{\varepsilon}\}^{\mathrm{T}}[\bar{\mathrm{C}}]\{\bar{\varepsilon}\})\,\mathrm{d}v - \int_S \{\delta\bar{\mathrm{u}}\}^{\mathrm{T}}\{\bar{\mathrm{T}}\}\,\mathrm{d}s\right)\mathrm{d}t = 0, \qquad [\bar{\mathrm{C}}] = \begin{bmatrix}[\mathrm{C}] & [\mathrm{e}]^{\mathrm{T}} \\ [\mathrm{e}] & -[\xi]\end{bmatrix}. \quad (7)$$

The infinitesimal strain relations are:

$$\varepsilon_{ij} = \tfrac{1}{2}(u_{i,j} + u_{j,i}), \qquad E_i = -\Phi_{,i} \quad (8)$$

Therefore by adopting appropriate elements and certain interpolating functions, displacements or voltage within an element can be expressed by nodal variables. Then by inserting equation (8) into equation (7), the finite element equation can be formulated.

3. FINITE ELEMENT MODEL

In order to clarify the cause of damage in composites induced by low velocity impact, it is necessary to analyze the whole impact procedure under the basis of three-dimensional elastic theory. On the other hand, it has been concluded from experiments that in low velocity impact, the damage tends to concentrate around the impact zone, especially in thick plates. Moreover, delamination is the major damage mode and its area is mainly related to the impact energy [12, 13]. As a result, complete 3-D analysis of the whole plate appears to be unnecessary. Here the plate is discretized by four different kinds of elements in three distinct regions (see Figure 1):

Region I: three-dimensional eight-node brick elements with incompatible modes. This region is in the vicinity of the impact point and is where damage is most likely to occur.

Region II: two-dimensional nine-node Lagrange plate elements. In this region, it is postulated that no damage exists.

Region III: transition elements.

In region I, eight-node brick elements with incompatible modes proposed by Wilson *et al*. [14] are utilized. The extended nodal displacements vector is:

$$\{\mathrm{q}^e\} = \{\delta_1^{(3)}, \ldots, \delta_8^{(3)}\}^{\mathrm{T}}, \qquad \{\delta_i^{(3)}\} = \{u_1, u_2, u_3, \Phi\}^{\mathrm{T}}, \qquad i = 1, 8 \quad (9)$$

and the displacements at any point within the element can be interpolated by the nodal displacements as:

$$u_a^{(3)} = \sum_{i=1}^{8} N_i^{(3)} u_{i\alpha}^{(3)} + \sum_{i=1}^{3} P_i a_{i\alpha}, \quad \alpha = 1, 4, \quad (10)$$

where $u_{i\alpha}^{(3)}$ is the extended nodal displacement and $P_i a_{i\alpha}$ is the incompatible mode. Generally, the piezoelectric layer must be insulated from the laminate; on the one hand, the finite element formulation is based on the continuity of displacements. Therefore, it is reasonable to let voltage $\Phi = 0$ if the node is on the interface between composite and piezoelectric layers.

Because the composites' high longitudinal to transverse modulus ratio often results in transverse shear deformation which cannot be neglected, Mindlin plate theory which takes transverse shear deformation into account is applied in region II and the displacements are described as:

$$u(x, y, z, t) = u_0(x, y, t) + z\theta_x(x, y, t), \qquad v(x, y, z, t) = v_0(x, y, t) + z\theta_y(x, y, t)$$
$$w(x, y, z, t) = w_0(x, y, t), \quad (11)$$

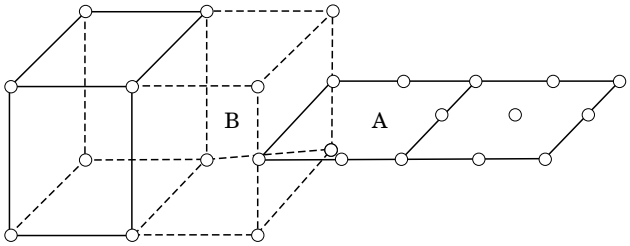

Figure 2. Transition elements: A, plate transition element; B, 3-D to 2-D transition element.

where u_0, v_0 and w_0 are midplane displacements, and θ_x, θ_y are rotational angles. It is also assumed that the voltage is linearly distributed through the thickness (Z-direction) of the piezoelectric layers:

$$\Phi(x, y, z, t) = (z - z_0)\beta(x, y, t) \tag{12}$$

where z_0 is the Z-coordinate of the bottom surface of each piezoelectric layer. Indeed $\beta(x, y, t)$ is the negative value of E_z. By adopting C^0 continuity nine-node Lagrange plate elements whose nodal displacements are

$$\{\mathrm{q}^e\} = \{\delta_1^{(2)}, \ldots, \delta_9^{(2)}\}, \qquad \{\delta_i^{(2)}\} = \{u_0, v_0, w_0, \theta_x, \theta_y, \beta\}^{\mathrm{T}}, \qquad i = 1, 9. \tag{13}$$

The corresponding displacements of any point in the midplane can be expressed by the nodal variables as

$$u_\alpha^{(2)}(x, y, t) = \sum_{i=1}^{9} N_i^{(2)} u_{i\alpha}^{(2)}(x, y, t), \qquad \alpha = 1, 6, \tag{14}$$

where $u_{i\alpha}^{(2)}$ is the extended nodal displacement.

In order to connect the above 3-D and 2-D elements smoothly, transition elements are indispensable. Here, two kinds of transition elements are introduced. Since there is no internode in the 3-D brick elements but the plate elements have, a "serendipity" plate element [15] as shown in Figure 2 (element A) which has no internode in the line that faces the 3-D element is developed. The shape functions of this kind of element can be established by the method suggested by Zienkiewicz [15].

A typical transition element between 3-D and 2-D regions is illustrated in Figure 2 (element B) in which the nodes on the face of the 3-D element adjoining the 2-D element are substituted by the corresponding nodes of the plate transition element. This transition region is firstly formed as an assembly of 3-D elements, and then after certain transformation and condensation to impose suitable constraints on the nodes located on the boundaries of the 2-D region, these nodes are converted so that they can be conveniently attached to the nodes of the 2-D elements. This procedure is formulated as follows:

Let $\{\mathrm{q}'\}$ denote global nodal displacements of the 3-D to 2-D transition elements before condensation, which is expressed as:

$$\{\mathrm{q}'\} = \{q_1^{(3)}, q_2^{(3)}\}^{\mathrm{T}}, \qquad \{q_1^{(3)}\} = \{\delta_1^{(3)}, \ldots, \delta_m^{(3)}\}^{\mathrm{T}}, \qquad \{q_2^{(3)}\} = \{\delta_{m+1}^{(3)}, \ldots, \delta_n^{(3)}\}^{\mathrm{T}}, \tag{15}$$

where $\{q_1^{(3)}\}$ denotes the degree of freedoms remaining unaltered and $\{q_2^{(3)}\}$ is the one to be modified. From equations (11) and (12), the following can be easily obtained:

$$\{\delta_i^3\} = [\mathrm{T}_i]\{\delta_r^{(2)}\}, \qquad i = m+1, n, \qquad [\mathrm{T}_i] = \begin{bmatrix} 1 & 0 & 0 & z_i & 0 & 0 \\ 0 & 1 & 0 & 0 & z_i & 0 \\ 0 & 0 & 1 & 0 & 0 & 0 \\ 0 & 0 & 0 & 0 & 0 & z_i - z_0 \end{bmatrix}, \quad (16)$$

where $\{\delta_i^{(3)}\}$, $\{\delta_r^{(2)}\}$ are expressed in equations (9) and (13) respectively and z_i is the Z-coordinate of the ith node.

Then the nodal displacement vector $\{\bar{q}\}$ of the transition elements after condensation is acquired as:

$$\{q'\} = [\mathrm{T}]\{\bar{q}\}, \qquad \{\bar{q}\} = \{q_1^{(3)}, q_2^{(2)}\}^{\mathrm{T}}, \qquad \{q_2^{(2)}\} = \{\delta_1^{(2)}, \ldots, \delta_p^{(2)}\}^{\mathrm{T}},$$

$$[\mathrm{T}] = \begin{bmatrix} I & 0 \\ 0 & T_I \end{bmatrix}, \qquad [\mathrm{T}_I] = \begin{bmatrix} T_{m+1} \\ \vdots \\ T_n \end{bmatrix}. \quad (17)$$

Now substituting equation (9–14) into equation (8), then into equation (7), the element mass and stiffness matrices for 2-D and 3-D elements can be assembled. In the transition region, for the serendipity elements, these matrices are established following the same procedure as the nine-node Lagrange elements. The 3-D to 2-D transition elements are firstly treated as 3-D elements, then after the condensation listed in equations (15–17), the stiffness and mass matrices are reduced to:

$$[\mathrm{K}''] = [\mathrm{T}]^{\mathrm{T}}[\mathrm{K}'][\mathrm{T}], \qquad [\mathrm{M}''] = [\mathrm{T}]^{\mathrm{T}}[\mathrm{M}'][\mathrm{T}] \quad (18)$$

where [K′] and [M′] are calculated with due consideration of the 3-D finite element process.

Consequently the global finite element equation is assembled as

$$[\mathrm{M}]\{\ddot{\mathrm{q}}\} + [\mathrm{K}]\{\mathrm{q}\} = \{\mathrm{F}\}, \quad (19)$$

where $\{\mathrm{q}\}$ is the extended global nodal displacements vector and $\{\mathrm{F}\}$ is the extended external force vector including contact force.

4. SOLUTION OF THE CONTACT FORCE

The external nodal force vector in equation (19) can be rewritten as:

$$\{\mathrm{F}\} = \{\mathrm{F}_1\} + \{\mathrm{F}_2\}, \qquad \{\mathrm{F}_1\} = F_s\{\mathrm{I}\}. \quad (20)$$

where $\{\mathrm{F}_1\}$ is assumed to be a point contact force vector, $\{\mathrm{I}\}$ is a unit vector whose components are zero except the one relative to the impact point. The point contact force F_s is expressed in reference [16] as:

Upon loading,

$$F = \kappa\alpha^{1.5}, \qquad \kappa = \tfrac{4}{3}\sqrt{r}\,[(1 - v_s^2)/E_s + 1/E_2]^{-1}. \quad (21)$$

Unloading,

$$F = F_m[(\alpha - \alpha_0)/(\alpha_m - \alpha_0)]^{2.5},$$

$$\alpha_0 = 0 \qquad \text{when } \alpha_m \leqslant \alpha_{cr}, \qquad \alpha_0 = \alpha_m[1 - (\alpha_{cr}/\alpha_m)^{2/5}] \qquad \text{when } \alpha_m > \alpha_{cr}. \tag{22}$$

Reloading,

$$F = F_m[(\alpha - \alpha_0)/(\alpha_m - \alpha_0)]^{1.5}. \tag{23}$$

In the above equations, α is the indentation depth (the distance between the impactor and the mid-surface of the plate), κ is the modified constant of the Hertz contact theory, r_s, v_s and E_s are the radius, Poisson ratio and Young's modulus of the isotropic impactor respectively, and E_2 is the transverse modulus normal to the fiber direction in the directly impacted layer. F_m is the maximum contact force just before unloading, α_m is the maximum indentation corresponding to F_m and α_0 is the permanent indentation during this loading/unloading process. α_{cr} is the critical indentation depth which is a material constant that can be determined from experiments.

Equation (19) is solved by the Newmark method. If Δt represents time increment, then at time $t + \Delta t$, equation (19) is converted to

$$[\bar{\mathrm{K}}]\{\mathrm{q}\}^{t+\Delta t} = F_s^{t+\Delta t}\{\mathrm{I}\} + \{\mathrm{F}_2\}^{t+\Delta t} + \{\mathrm{P}\}^t, \tag{24}$$

where [K] and $\{\mathrm{P}\}^t$ are determined by the Newmark method, $F_s^{t+\Delta t}$ is the contact force at time $t + \Delta t$ which is decided in equations (21–23) by the indentation depth $\alpha^{t+\Delta t}$

$$\alpha^{t+\Delta t} = w_s^{t+\Delta t} - w_c^{t+\Delta t} \tag{25}$$

where $w_s^{t+\Delta t}$ and $w_c^{t+\Delta t}$ are displacements of the impactor and the point in the mid surface of the plate at the impacting direction. $w_s^{t+\Delta t}$ along with the impactor's velocity v_s is solved from equation (26)

$$v_s^{t+\Delta t} = v_0 - \frac{1}{m_s}\int_0^{t+\Delta t} F_s(\tau)\,\mathrm{d}\tau, \qquad w_s^{t+\Delta t} = v_0(t+\Delta t) - \frac{1}{m_s}\int_0^{t+\Delta t} F_s(\tau)(t+\Delta t-\tau)\,\mathrm{d}\tau \tag{26}$$

Since only the linear terms are considered in the basic equations, with the linear superimposing law, the following can be easily obtained:

$$\{\mathrm{q}\}^{t+\Delta t} = F_s^{t+\Delta t}\{\mathrm{q}\}_1^{t+\Delta t} + \{\mathrm{q}\}_2^{t+\Delta t}, \qquad w_c^{t+\Delta t} = F_s^{t+\Delta t}w_1^{t+\Delta t} + w_2^{t+\Delta t} \tag{27}$$

where $\{\mathrm{q}\}_1^{t+\Delta t}w_1^{t+\Delta t}$ are caused by unit contact force at time $t + \Delta t$, and $\{\mathrm{q}\}_2^{t+\Delta t}w_2^{t+\Delta t}$ result from $\{F_2\}^{t+\Delta t} + \{P\}^t$. Substituting equations (25–27) into equations (21–23), the expressions of the contact force at time $t + \Delta t$ are obtained:

during loading

$$F_s^{t+\Delta t} = \kappa\left[v_0(t+\Delta t) - \frac{1}{m_s}\int_0^{t+\Delta t} F_s(\tau)(t+\Delta t-\tau)\,\mathrm{d}\tau - F_s^{t+\Delta t}w_1^{t+\Delta t} - w_2^{t+\Delta t}\right]^{1.5}, \tag{28}$$

during unloading

$$F_s^{t+\Delta t} = F_m\left[\frac{v_0(t+\Delta t) - \frac{1}{m_s}\int_0^{t+\Delta t} F_s(\tau)(t+\Delta t-\tau)\,\mathrm{d}\tau - F_s^{t+\Delta t}w_1^{t+\Delta t} - w_2^{t+\Delta t} - \alpha_0}{\alpha_m - \alpha_0}\right]^{2.5}, \tag{29}$$

during reloading

$$F_s^{t+\Delta t} = F_m \left[\frac{v_0(t+\Delta t) - \dfrac{1}{m_s}\displaystyle\int_0^{t+\Delta t} F_s(\tau)(t+\Delta t-\tau)\,\mathrm{d}\tau - F_s^{t+\Delta t} w_1^{t+\Delta t} - w_2^{t+\Delta t} - a_0}{\alpha_m - \alpha_0} \right]^{1.5}. \tag{30}$$

With regard to the integral term $\int_0^{t+\Delta t} F_s(\tau)(t+\Delta t-\tau)\,\mathrm{d}\tau$ in the above equations, since $F_s(\tau)$ is unknown in the time interval t–$(t+\Delta t)$, a linear interpolation of $F_s(\tau)$ during t–$(t+\Delta t)$ is introduced,

$$F_s(\tau) = F_s^t + (F_s^{t+\Delta t} - F_s^t)(\tau - t)/\Delta t, \qquad t < \tau \leqslant t + \Delta t. \tag{31}$$

Inserting equation (31) into equations (28–30), $F_s^{t+\Delta t}$ can be rewritten as:

during loading

$$F_s^{t+\Delta t} = \kappa \left[v_0(t+\Delta t) - \frac{1}{m_s}\int_0^t F_s(\tau)(t+\Delta t-\tau)\,\mathrm{d}\tau - \frac{F_s^t \Delta t^2}{3m_s} - \frac{F_s^{t+\Delta t}\Delta t^2}{6m_s} - F_s^{t+\Delta t} w_1^{t+\Delta t} - w_2^{t+\Delta t} \right]^{1.5}, \tag{32}$$

during unloading

$$F_s^{t+\Delta t} = F_m \left[\left(v_0(t+\Delta t) - \frac{1}{m_s}\int_0^t F_s(\tau)(t+\Delta t-\tau)\,\mathrm{d}\tau - \frac{F_s^t \Delta t^2}{3m_s} - \frac{F_s^{t+\Delta t}\Delta t^2}{6m_s} - F_s^{t+\Delta t} w_1^{t+\Delta t} - w_2^{t+\Delta t} - \alpha_0 \right) \Big/ (\alpha_m - \alpha_0) \right]^{2.5}, \tag{33}$$

during reloading

$$F_s^{t+\Delta t} = F_m \left[\left(v_0(t+\Delta t) - \frac{1}{m_s}\int_0^t F_s(\tau)(t+\Delta t-\tau)\,\mathrm{d}\tau - \frac{F_s^t \Delta t^2}{3m_s} - \frac{F_s^{t+\Delta t}\Delta t^2}{6m_s} - F_s^{t+\Delta t} w_1^{t+\Delta t} - w_2^{t+\Delta t} - \alpha_0 \right) \Big/ (\alpha_m - \alpha_0) \right]^{1.5}, \tag{34}$$

The above equations are solved by the following process: If $F_s^{t+\Delta t} = 0$, $\{\mathrm{q}\}_2^{t+\Delta t}$ and $w_2^{t+\Delta t}$ can be solved from equation (24); then solve again to obtain $\{\mathrm{q}\}_1^{t+\Delta t}$ and $w_1^{t+\Delta t}$ by letting $\{\mathrm{P}\}^t = 0$, $\{F_2\}^{t+\Delta t} = 0$, $F_s^{t+\Delta t} = 1$; finally, using the Newton Raphson method to solve the non-linear equations (31–34), $F_s^{t+\Delta t}$ is acquired. The nodal displacements are determined by equation (27).

5. SENSOR EQUATION

The impact-induced strain is monitored by the piezoelectric sensors. The closed circuit charge signal measured from the surface electrode to the force field is [1–2]

$$q(t) = \tfrac{1}{2}\left[\left(\int_A D_3\,\mathrm{d}A \right)_{z=z_0} + \left(\int_A D_3\,\mathrm{d}A \right)_{z=z_1} \right], \tag{35}$$

where A is the effective electrode surface area of each sensor, z_0 and z_1 are the Z-Co-ordinates of the bottom and top surface of the piezoelectric layer respectively. Assuming there is no external surface charge on the piezoelectric sensors and the charge results from mechanical strain, D_3 is determined from equation (3) as:

$$D_3 = \{e_3\}\{\varepsilon\}, \qquad \{e_3\} = \{e_1, e_{32}, e_{33}, e_{34}, e_{35}, e_{36}\} \tag{36}$$

The piezoelectric layers are also discretized by 3-D or 2-D elements depending on their location. Accordingly, the charge generated on each electrode surface is calculated as:

$$q(t) = \sum_{i=1}^{N_s^{(3)}} \int_{A_i^{(3)}} \{e_3\}\{\mathrm{B}^{(3)}]\{\mathrm{q}^e\}_i \, \mathrm{d}A, \qquad \text{3-D region,} \tag{37}$$

$$q(t) = \sum_{i=1}^{N_s^{(2)}} \int_{A_i^{(2)}} \{e_3^{(2)}\}[\mathrm{B}^{(2)}]\{\mathrm{q}^e\}_i \, \mathrm{d}A, \qquad \{e_3^{(2)}\} = \{e_{31}, e_{32}, e_{34}, e_{35}, e_{36}\}, \qquad \text{2-D region,} \tag{38}$$

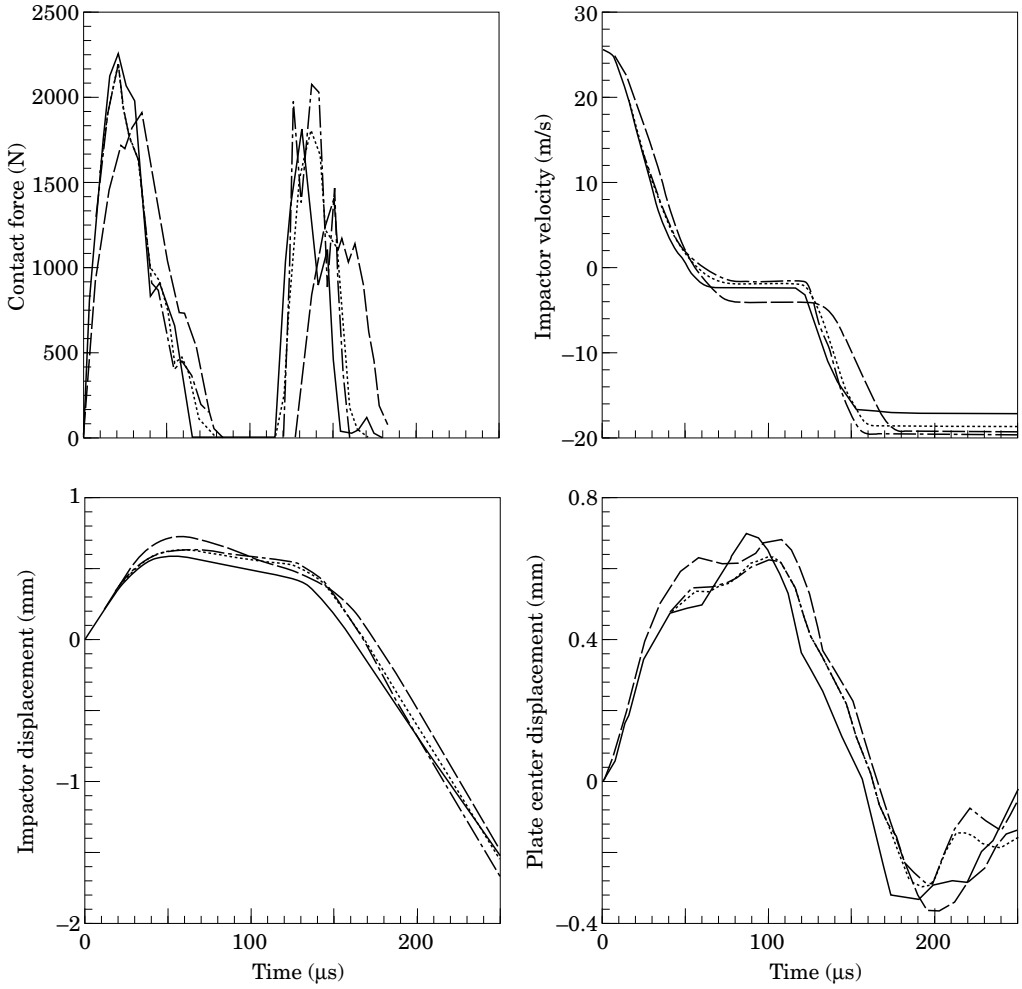

Figure 3. Comparison of results for various elements. ——, Wu result; – – –, 2-D elements; · · · ·, 3-D elements; – · – mixed elements.

TABLE 1

Material properties of composite reference [8] *and PVDF reference* [17]

	Composite	PVDF
Longitudinal Young's modulus, E_1 (GPa)	145·5	2·0
Transverse Young's modulus, E_2 (GPa)	10·0	2·0
Shear modulus in 1-, 2-direction, G_{12} (GPa)	5·687	0·775
Shear modulus in 2-, 3-direction, G_{23} (GPa)	3·85	0·775
Poisson ratio in 1-, 2-direction, v_{12}	0·3	0·29
Density, ρ (kg/m^3)	1535·4	1800·0
Layer thickness, h (mm)	0·16	0·1
Critical indentation, α_{cr} (mm)	0·08	–
Piezoelectric strain constant, d_{31} (pm/v)	–	23·0
Piezoelectric strain constant, d_{33} (pm/v)	–	−33·0

where the superscription (2) and (3) denote the element type, N_s is the number of elements into which the sensor is divided, A_i is the effective electrode surface area of the ith element, $\{q^e\}_i$ is the nodal displacement vector which is obtained by eliminating nodal electric variables in equation (9) or equation (13) and the definition of [B] can be found in the appendix. Equations (37–38) are computed using Gauss integral law.

Because the piezoelectric effect of PVDF film is directional, it can be expected that by changing the skew angle θ which is the angle between the X co-ordinate and its pole direction 1 (see Figure 1), various motions such as bending, stretching and torsion are displayed from the sensor charge signal in different combinations due to the relationship between [e] and θ:

$$[\mathrm{e}] = [\mathrm{A}][\mathrm{e}^0][\mathrm{T}]^{\mathrm{T}}, \qquad [\mathrm{A}] = \begin{bmatrix} \cos\theta & -\sin\theta & 0 \\ \sin\theta & \cos\theta & 0 \\ 0 & 0 & 1 \end{bmatrix},$$

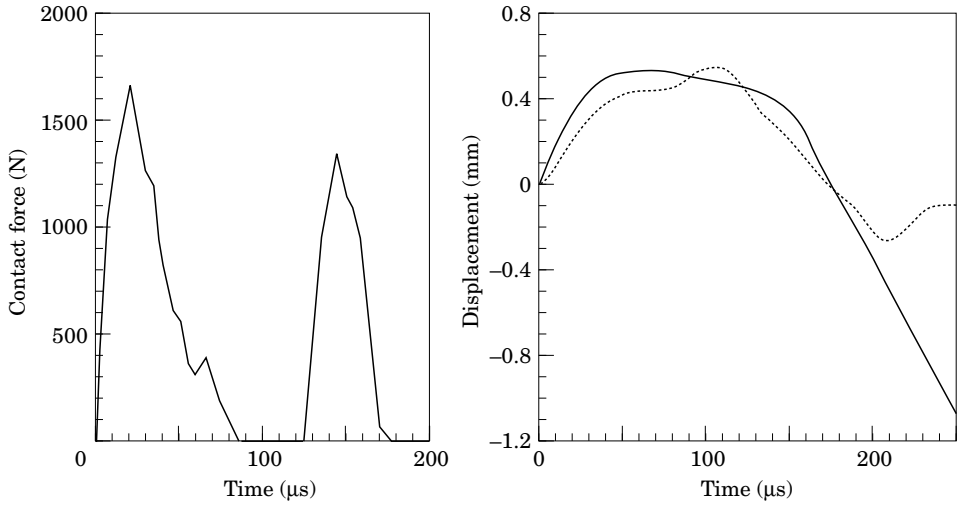

Figure 4. History of contact force and displacement. ——, impactor; · · · · , plate center.

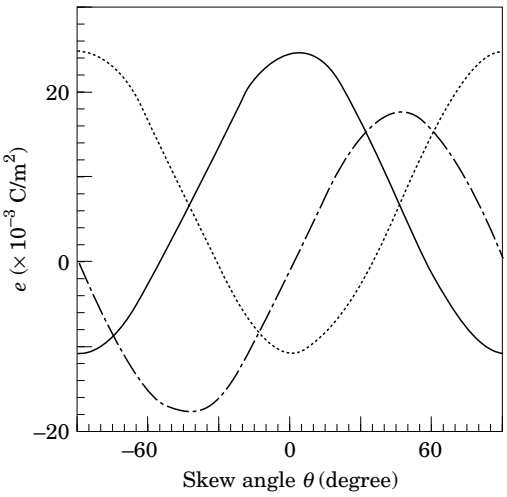

Figure 5. Piezoelectric stress/charge constants of PVDF film versus skew angle. ——, e_{31}; · · · ·, e_{32}; – · –, e_{34}.

$$[\mathrm{T}] = \begin{bmatrix} \cos^2\theta & \sin^2\theta & 0 & -2\sin\theta\cos\theta & 0 & 0 \\ \sin^2\theta & \cos^2\theta & 0 & 2\sin\theta\cos\theta & 0 & 0 \\ 0 & 0 & 1 & 0 & 0 & 0 \\ \sin\theta\cos\theta & -\sin\theta\cos\theta & 0 & \cos^2\theta - \sin^2\theta & 0 & 0 \\ 0 & 0 & 0 & 0 & \cos\theta & -\sin\theta \\ 0 & 0 & 0 & 0 & \sin\theta & \cos\theta \end{bmatrix} \tag{39}$$

where $[e^0]$ is the original piezoelectric stress constants in 1-, 2-, 3-axes and determined in equation (4).

6. NUMERICAL EXAMPLES

In order to verify the present method, a numerical example previously calculated by Wu [8] is analyzed and a comparison between the two results is made.

Consider a square plate with a ply orientation of $[0^\circ/-45^\circ/45^\circ/90^\circ]_{2s}$ which is rigidly fixed on its four edges and subjected to an impact at a velocity of 25·4 m/s (1000 in/s) reference [8]. Because of symmetry, only one quarter of the plate is studied and the calculations are carried out using an $8 \times 8 \times 4$ 3-D mesh, 8×8 2-D mesh, and mixed elements consisting of $3 \times 3 \times 4$ 3-D mesh in the inner part (see Figure 1), respectively. The history of contact force, impactor's velocity and displacement, and plate center displacement are depicted in Figure 3. A certain difference exists between Wu's results [8] and those obtained by the $8 \times 8 \times 4$ 3-D mesh. This is due to the coarse mesh and the simplification of contact force adopted in [8]. For the 2-D plate element results, the discrepancy is distinctive which suggests that in analyzing an impact problem, it is not accurate enough to utilize solely two-dimensional plate theory because of its simplification of the displacements as can be seen in equation (11). Most importantly, as shown in the figures, in contrast to results using only two-dimensional elements, the results computed by the mixed elements agree well with those obtained by the $8 \times 8 \times 4$ 3-D mesh.

Using the present mixed elements, a 16-ply $[0_2^\circ/90_2^\circ/+45_2^\circ/-45_2^\circ]_s$ square laminate with clamped edges subjected to impact of an aluminum sphere with a diameter of 12·7 mm

at a speed of 20 m/s is investigated and the dynamic impact induced strain during the contact duration is simultaneously monitored by sensors made from PVDF film which are surface mounted on the side opposite the impact. The finite element mesh is shown in Figure 1 ($l_1 = 15$ mm, $l_2 = 20$ mm and region I is discretized by $3 \times 3 \times 4$ 3-D elements). The material properties are listed in Table 1. The dimensions of the laminate and each piezoelectric sensor are $80\text{ mm} \times 80\text{ mm}$ and $10\text{ mm} \times 10\text{ mm}$ respectively, and the locations of the piezoelectric sensors are illustred in Fig. 1—Sensor A is modelled by 3-D element while sensor B and C by 2-D ones. The time increment Δt in the calculations is chosen as 5 μs which is found to be appropriate for convergence, and the results are presented in Figures 4–8.

The contact force, displacements of the impactor at the center of the plate during impact are shown in Figure 4. It is found that the bonded PVDF patches have very little effect on the laminate's dynamic response, which can be attributed to the flexibility of PVDF film and which proves to be an ideal sensor. The dependence of the piezoelectric stress

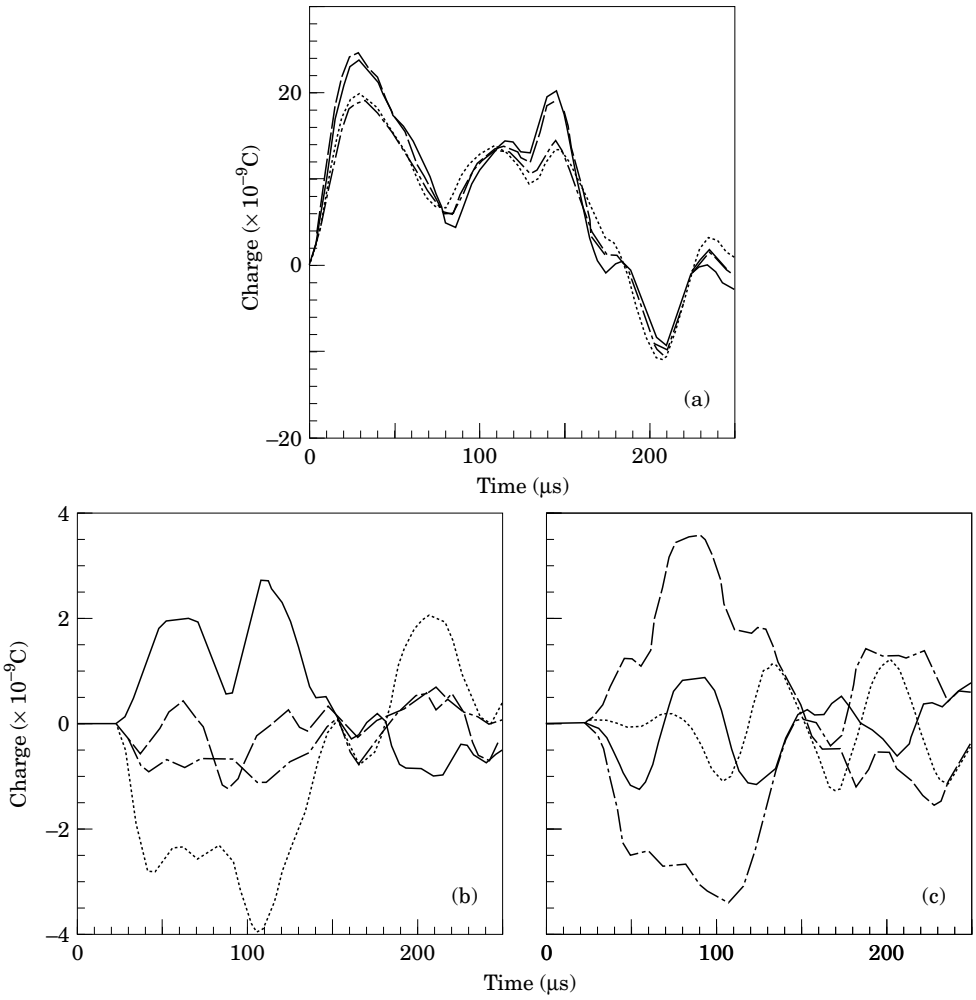

Figure 6. Charge generated by piezoelectric sensors: (a) sensor A; (b) sensor B; (c) sensor C. Skew angle θ^0: ——, −90; – – –, −45; · · · · ·, 0; – · – · –, 45.

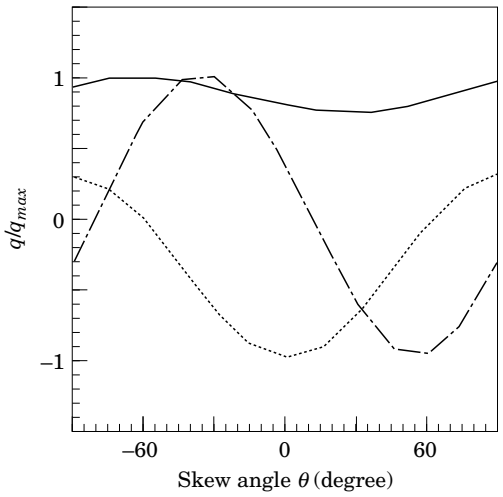

Figure 7. Normalized charge of piezoelectric sensors versus skew angle. Sensors: ——, A; · · · ·, B; – · – ·, C.

constants, e on skew angle is demonstrated in Figure 5, and the closed circuit charge q measured from the piezoelectric sensors as functions of time is presented in Figure 6. The influence of the skew angle θ can be seen from the figures as well and the variation of the normalized charge $q/|q|_{\max}$ with the skew angle θ at time $t = 30$ μs is presented in Figure 7. In order to compare the charge signal generated by piezoelectric sensors with the local strain which the sensors are intended to monitor, four components of the strain, i.e. ε_x, ε_y, ε_z and γ_{xy} at (1·06 mm, 1·06 mm, 1·28 mm) as functions of time are depicted in Figure 8.

As can be seen, the charge curve vividly manifests the combinations of the strain components and the piezoelectric constants can be regarded as weighted factors. With different skew angles θ, these weighted factors are changed and different combinations of the strain components are achieved which are clearly reflected by the output charge signal. In addition, Figure 7 shows that the charge reaches a maximum value at a certain skew angle θ which suggests that the charge may not reach this maximum value when $\theta = 0$, often used in normal cases, but other values of θ can engender much larger ones that are more easily detected. This indicates that changing θ can improve the sensors' sensitivity.

7. CONCLUDING REMARKS

The feasibility of using piezoelectric sensors to measure strain in composite induced by low velocity foreign impact is investigated numerically. This is achieved by a mixed finite elements approach: in the vicinity of the impact point, three-dimensional finite elements are adopted while in the rest of the plate, two-dimensional plate elements are introduced and a transition region including two kinds of transition elements provides a smooth link between these two types of elements. This methodology is based on the fact that in the former part where damage is most likely to occur, three-dimensional analysis is indispensable but in the latter, two-dimensional analysis is enough. Numerical examples prove the effectiveness and efficiency of this method. In addition, by linear interpolation, the contact force can be calculated more accurately.

The close circuit charge generated by the piezoelectric sensors is computed as well, and the results show that it can manifest the impact-induced strain. Further computations

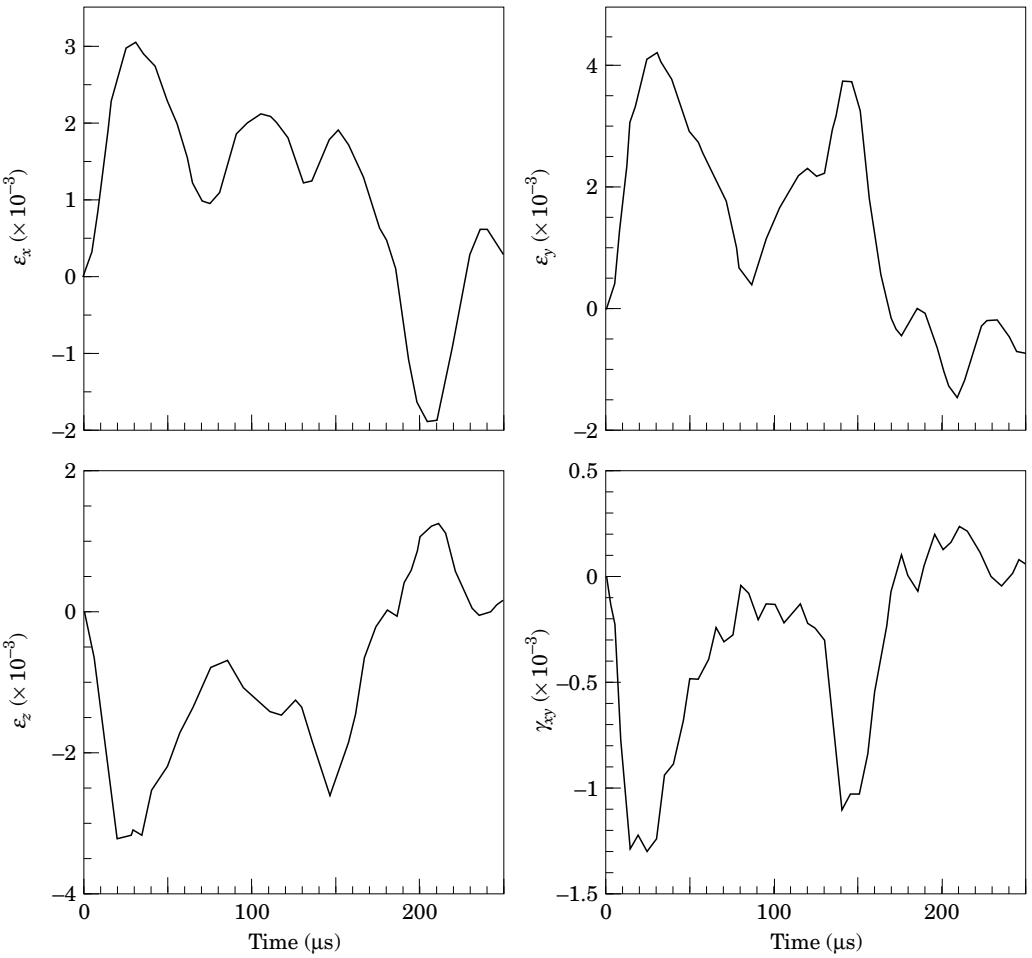

Figure 8. Strain history.

suggest that the PVDF sensor's output depends heavily on the skew angle. This means that by changing the skew angle not only a maximum output can be obtained, but also the contribution of each strain component can be predicted, and hence the level of different stress components.

REFERENCES

1. C. K. Lee 1990 *J. Acoust. Soc. Am.* **87**(3), 1144–1158. Theory of laminated piezoelectric plates for the design of distributed sensors/actuators. Part I: governing equations and reciprocal relationships.
2. C. K. Lee and F. C. Moon 1990 *Journal Applied Mechanics* **57**, 434–441. Modal sensors/actuators.
3. L. Yin, X.-M. Wang and Y.-P. Shen 1995 *Computers and Structures*. Damage monitoring in composite laminates by piezoelectric films. [To be published].
4. C. T. Sun and S. Chattopadhyay 1975 *Journal of Applied Mechanics* **42**, 693–698. Dynamic response of anisotropic laminated plates under initial stress to impact of a mass.
5. R. L. Ramkumar and P. C. Chen 1983 *AIAA Journal* **21**, 1448–1452. Low-velocity impact response of laminated plates.

6. C. T. Sun and J. K. Chen 1985 *Journal of Composite Materials* **19**, 490–504. On the impact of initially stressed composite laminates.
7. J. D. Lee, S. Du and H. Liebowitz 1984 *Computers and Structures* **19**, 807–813. Three dimensional finite element and dynamic analysis of composite laminate subjected to impact.
8. H. T. Wu and F. K. Chang 1989 *Computers and Structures* **31**, 453–466. Transient dynamic analysis of laminated composite plates subjected to transverse impact.
9. P. Pojanasomboon, S. E. Watkins and K. Chandrashekhara 1994 *Proceedings of ICIM'94*, 985–993. Strain sensing of low velocity impacts for smart composite plates.
10. K. S. Surana 1980 *International Journal for Numerical Methods in Engineering* **15**, 991–1020. Transition finite elements for three-dimensional stress analysis.
11. C. G. Shah and A. V. Krishnamurty 1991 *Computers and Structures* **39**, 231–242. Analysis of edge delamination in laminates through combined use of quasi-three-dimensional, eight-noded, two-noded and transition elements.
12. H. T. Wu and G. S. Springer 1988 *Journal of Composite Materials* **22**, 518–532. Measurements of matrix cracking and delamination caused by impact on composite plates.
13. S. Hong and D. Liu 1989 *Experimental Mechanics* **29**, 115–120. On the relation between impact energy and delamination area.
14. E. L. Wilson, R. L. Taylor, W. P. Doherty and J. Ghaboussi 1973 *Numerical and Computer Methods in Structural Mechanics* (Ed. S. J. Fenves *et al*.), New York: Academic Press. 43–57. Incompatible displacement models.
15. O. C. Zienkiewicz 1977 *The Finite Element Method* (3*rd edition*), London: McGraw-Hill.
16. T. M. Tan and C. T. Sun 1985 *Journal of Applied Mechanics* **52**, 6–12. Use of statical indentation laws in the impact analysis of laminated composite plates.
17. M. V. Grandhi, B. S. Chan and P. Joshi 1992 *Smart Materials and Structures*, London: Chapman & Hall.

APPENDIX

The matrices $[B^{(3)}]$ and $[B^{(2)}]$ in eqs. (37, 38) are:

$$[B^{(3)}] = [B'][G][K]_{aa}^{-1}[K]_{aq}, \qquad [B'] = [B'_1, B'_2, \ldots, B'_8], \qquad [G] = [G_1, G_2, G_3],$$

$$[B'_i] = \begin{bmatrix} N^{(3)}_{i,x} & 0 & 0 \\ 0 & N^{(3)}_{i,y} & 0 \\ 0 & 0 & N^{(3)}_{i,z} \\ N^{(3)}_{i,y} & N^{(3)}_{i,x} & 0 \\ N^{(3)}_{i,z} & 0 & N^{(3)}_{i,x} \\ 0 & N^{(3)}_{i,z} & N^{(3)}_{i,y} \end{bmatrix}, \qquad [G_i] = \begin{bmatrix} p_{i,x} & 0 & 0 \\ 0 & p_{i,y} & 0 \\ 0 & 0 & p_{i,z} \\ p_{i,y} & p_{i,x} & 0 \\ p_{i,z} & 0 & p_{i,x} \\ 0 & p_{i,z} & p_{i,y} \end{bmatrix}$$

$$[K_{aa}] = \int_V [G]^T[C][G]\,dv, \qquad [K_{aq}] = \int_V [G]^T[C][B]\,dv,$$

$$[B^{(2)}] = [B^{(2)}_1, B^{(2)}_2, \ldots, B^{(2)}_g],$$

$$[B^{(2)}_i] = \begin{bmatrix} N^{(2)}_{i,x} & 0 & 0 & zN^{(2)}_{i,x} & 0 \\ 0 & N^{(2)}_{i,y} & 0 & 0 & zN^{(2)}_{i,y} \\ N^{(2)}_{i,y} & N^{(2)}_{i,x} & 0 & zN^{(2)}_{i,y} & zN^{(2)}_{i,x} \\ 0 & 0 & N^{(2)}_{i,x} & N^{(2)}_{i} & 0 \\ 0 & 0 & N^{(2)}_{i,y} & 0 & N^{(2)}_{i} \end{bmatrix}.$$